Journal of Power Sources 196 (2011) 7639–7644

Contents lists available at ScienceDirect

Journal of Power Sources

journal homepage: www.elsevier.com/locate/jpowsour

Effect of alumina on the curvature, Young's modulus, thermal expansion coefficient and residual stress of planar solid oxide fuel cells

Chang Rong He, Wei Guo Wang*, Jianxin Wang, Yejian Xue

Division of Fuel Cell and Energy Technology, Ningbo Institute of Materials Technology and Engineering, Chinese Academy of Sciences, 519 Zhuangshi Road, Ningbo 315201, PR China

ARTICLE INFO

Article history:
Received 6 April 2011
Received in revised form 9 May 2011
Accepted 12 May 2011
Available online 19 May 2011

Keywords:
Solid oxide fuel cell
Curvature
Young's modulus
Thermal expansion coefficient
Residual stress

ABSTRACT

Planar solid oxide fuel cells (SOFCs) are composites consisting of porous and dense functional layers as electrodes and electrolytes, respectively. Because of the thermo-elastic mismatch between the individual layers, residual stresses develop during manufacturing and cause unconstrained cells to warp. The addition of alumina decreases the thermal expansion coefficient (TEC) of the NiO and yttria-stabilized zirconia (YSZ) anode-support material. Correspondingly, the lower TECs have flattened the half cells during fabrication. In addition, the residual stress at room temperature (RT) for samples with more than 4 wt% alumina is only 20% of the residual stress of the samples without alumina, at approximately 100 MPa. The effects of Al_2O_3 on the curvature, Young's modulus, TEC and residual stress of the SOFC with $(NiO–YSZ)_{1-x}(Al_2O_3)_x$ (x = 1–5 wt%) anode support are discussed in this work.

1. Introduction

The operation of SOFC components at temperatures of 700–800 °C and the need for thermal cycling between room and operating temperature generates interest in mechanical aspects, related to the influence of temperature on the curvature behavior of planar cells. Furthermore, the thermo-elastic properties of SOFC materials and components are receiving increased attention due to efforts to scale up the cells and improve the long-term performance.

Likewise, anode-supported SOFCs have recently received a great deal of interest [1–5]. Typical anode-supported cells have a thin and dense electrolyte membrane (typically 15 μm thick) supported on a porous cermet anode (typically 400 μm thick). The support is usually made with a porous composite of NiO and yttria-stabilized zirconia (YSZ), co-sintered with the YSZ membrane at high temperature (e.g., 1,350 °C), followed by reducing the NiO–YSZ anode to Ni–YSZ at the operating temperature. This material is preferred because of its good electronic conductivity, chemical and structural stability, catalytic properties and compatibility with other materials in SOFC [6]. Because the support has a higher thermal expansion coefficient (TEC) than the electrolyte, the electrolyte is placed in compression and the support in tension when they are cooled. As a result, the TEC mismatch induces a large residual stress in the cell at room temperature (RT) [7–10]. The stress distribution also causes the structure to bend due to asymmetry. The porous cathode (typically a 20-μm thick composite of strontium-doped lanthanum manganite and YSZ) is then applied onto the electrolyte and sintered at a moderate temperature (e.g., 1,100 °C). Because of its low stiffness, the cathode has little effect on the stresses in the other components.

The thermal stress may induce micro-cracks or cause delamination of the electrolyte at the interface under a thermal cycle. These damages of the cell can decrease the cell performance and sometimes destroy the cell.

In this paper, it was shown that adding Al_2O_3 in the NiO–YSZ support materials for the SOFC affected the TEC mismatch and reduced the residual stress in the cell.

2. Experimental

The Al_2O_3–Ni–YSZ anode was produced from high purity NiO (>99.99%), Al_2O_3 powders (with approximately 10–20 nm particle size) and commercial 3 mol% Y_2O_3 stabilized ZrO_2 (3YSZ, TOSOH Corp.). Green samples containing 95–100 wt% (3YSZ–NiO, 50:50 wt%) with 0–5 wt% Al_2O_3 were prepared by the tape casting method.

SOFC half cells (fuel cells without a cathode) were used for the curvature studies of the residual stress. The half cells were comprised of an approximately 400-μm thick, porous Al_2O_3–Ni–YSZ anode substrate and an approximately 10-μm thick 8 mol% Y_2O_3 stabilized ZrO_2 electrolyte (8YSZ, TOSOH Corp.). The curvatures of the samples were tested by a residual stress tester (JLCST022, J&L

* Corresponding author. Tel.: +86 574 8791 1363; fax: +86 574 8668 5846.
E-mail address: WGWang@nimte.ac.cn (W.G. Wang).

0378-7753/$ – see front matter © 2011 Elsevier B.V. All rights reserved.
doi:10.1016/j.jpowsour.2011.05.025

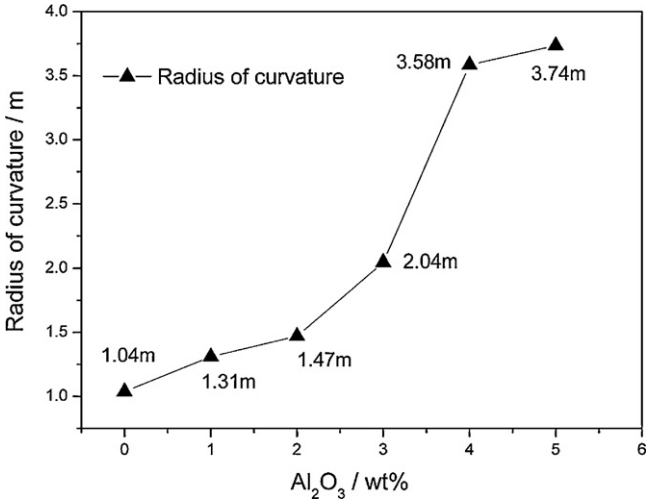

Fig. 1. Radius of curvature as a function of alumina content before H_2 reduction.

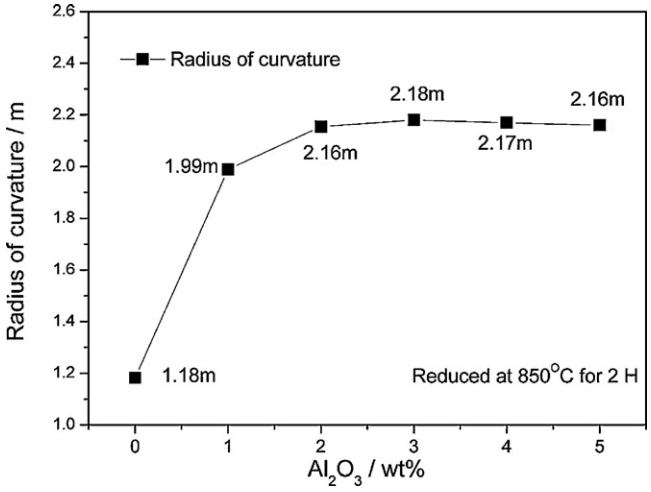

Fig. 2. The increase in the radius of curvature for the half cell as alumina content increased after reduction.

Tech Corp.) using 4-mm × 40-mm specimens that were laser cut and polished after they were sintered at 1,350 °C in air for 4 h. Approximately half of the samples were reduced in H_2 at 850 °C for 2 h. The residual stresses at room temperature were estimated from the curvature of the laminates and the elastic constants of the individual layers.

For Young's modulus measurements, anode specimens with the dimensions of 4 mm × 1.4 mm × 36 mm were prepared and polished after they were sintered at 1,350 °C in air for 4 h, and half of the samples were reduced in H_2 at 850 °C for 2 h. More than 10 specimens were measured to acquire average values of Young's modulus, and the thickness of each specimen was determined by a micrometer caliper. Young's modulus (E) was measured by the three-point bending test and calculated by the following equation:

$$E = \frac{3L(P_2 - P_1)}{2bh^2(\varepsilon_2 - \varepsilon_1)} \quad (1)$$

where E is Young's modulus (GPa), P_1 and P_2 are the loads at the beginning and end points of the bending test (N), L is the span length (mm), b is the width of the specimen (mm), h is the thickness of the specimen (mm) and ε_1 and ε_2 are the strain at P_1 and P_2.

The specimens were tested using an Instron machine (Model 5567) according to the testing method GB/T 10700-2006 [11] with a cross-head speed of 0.3 mm min^{-1}. The linear TECs of the Ni–YSZ anode supports with 0–5 wt% Al_2O_3 before and after H_2 reduction (NiO–YSZ and Ni–YSZ, respectively) were measured using a pushrod dilatometer (PCY-b TEC testing equipment, Xiangtan, China) and an alumina standard in the temperature range from 20 to 800 °C. All samples were cut into bars ~30 mm in length with varying cross-sectional dimensions, depending on the specimens. The Ni–YSZ anode specimens reduced with H_2 were measured in a nitrogen atmosphere, whereas all the others were measured in air. The heating/cooling rate was 1 K min^{-1}.

3. Results and discussion

The residual stresses in multilayers produced at high temperatures by either co-sintering or diffusion bonding are derived primarily from the misfit in thermal expansion. The stresses are relatively uniform with minimal gradients through the layers, and bending in multilayers occurs because of the moments of stress associated with the residual field. The residual stresses at RT can be estimated from the curvature of the laminates and the elastic constants of the individual layers, as expressed by [10,12]:

$$\sigma_r^* = \frac{E_2 h_2^2}{R6h_1(1-\nu)} \quad (2)$$

where E_2 denotes Young's modulus of the anode, h_1 and h_2 denote the thicknesses of the electrolyte layer and anode layer, respectively, R denotes the radius of curvature and ν denotes Poisson ratio.

To evaluate the residual stresses, the radius of curvature of the samples, the elastic modulus of the anode substrate and the thickness of each layers were used.

3.1. Radius of curvature of the half cells before and after H_2 reduction

The radius of curvature study revealed that the addition of alumina increase the radius of curvature of the half cells during fabrication. The radius of curvature increased non-linearly with increasing alumina content both before and after H_2 reduction, as shown in Figs. 1 and 2. The mean radius of curvature of the unreduced half cell without alumina was 1.04 m. When the alumina content increased to more than 3 wt%, the radius of curvature increased rapidly up to 2.04 m. When the alumina content was 5 wt%, the radius of curvature increased to 3.74 m. After H_2 reduction at 850 °C for 2 h, the radius of curvature for all the samples with alumina increased to more than 1.99 m. When the alumina

Table 1
Linear, exponential and non-linear correlations for Young's modulus vs. porosity for the NiO–YSZ composites.

	Correlation of E		b	E_o
For NiO–YSZ				
Linear	$E = E_o(1 - bp)$	(3)	2.10	205
Exponential	$E = E_o \exp(-bp)$	(4)	2.48	207
Non-linear	$E = E_o[1 - bp/(1 + (b - 1)p)]$	(5)	2.55	207
For Ni–YSZ	$E = E_o(1 - bp)$	(6)	1.756	206

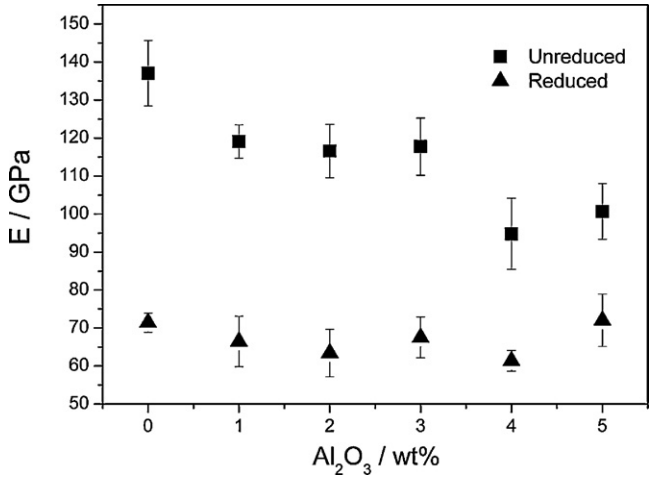

Fig. 3. Young's modulus of as-sintered NiO–YSZ–Al_2O_3 or Ni–YSZ–Al_2O_3 composites as a function of alumina content.

content was higher than 2 wt%, the radius of curvature became constant at approximately 2.16 m. After H_2 reduction, the half cell with 3 wt% alumina was flatter than the one without alumina and had the lowest change in radius of curvature in this study, from 2.04 to 2.18 m.

3.2. Young's modulus of the anode supports before and after H_2 reduction

Young's modulus measured at RT for the anode supports before and after H_2 reduction is shown in Fig. 3. Different correlations between the dependencies of elastic properties and porosity have been reported in the literature. Atkinson and Selcuk [13] referred to work from different authors and gave three correlations for the oxidized NiO–YSZ composite. These linear, exponential and non-linear correlations are summarized in Table 1. Measured values of the sample without alumina are compared with results reported in the literature [14] and those calculated by the three correlations in Table 2. It could be seen that the measured values agreed well with the data from the literature [14], but they were slightly lower than those calculated by the three correlations.

As the alumina content increased, Young's modulus decreased gradually, as shown in Fig. 3. Young's modulus was approximately 120 GPa when the alumina content was less than 3 wt% and approximately 100 GPa at 4 and 5 wt% prior to H_2 reduction. After H_2 reduction, Young's modulus became approximately 60–75 GPa because all samples had approximately 35% open porosity.

3.3. Effect of alumina on TEC of the anode supports

A simple model often used for TEC calculation is Turner's model [15,16]. The model assumes homogeneous strain throughout the composite, and only uniform hydrostatic stresses exist in the composite phases. The stresses are assumed to be insufficient to disrupt the composite. Each component in the composite is constrained to change dimensions with temperature at the same rate as the composite, and the shear deformation is negligible. Using a balance of internal average stresses, Turner derived the TEC of two-component composite as follows:

$$\alpha_c = \frac{\alpha_1 V_1 k_1 + \alpha_2 V_2 k_2}{V_1 k_1 + V_2 k_2} \quad (7)$$

where α is the TEC, V is the volume fraction of the solid phases and K is their bulk modulus.

Table 2
Measured Young's modulus compared with the literature values under linear, exponential and non-linear correlations.

	$E_{NiO-YSZ}$ (GPa)/porosity (%)	E_{Ni-YSZ} (GPa)/porosity (%)
This work	137/12	71/35
Literature [14]	127/around 18	73/38
Calculated by (3)	154/12	
Calculated by (4)	154/12	
Calculated by (5)	154/12	
Calculated by (6)		79/35

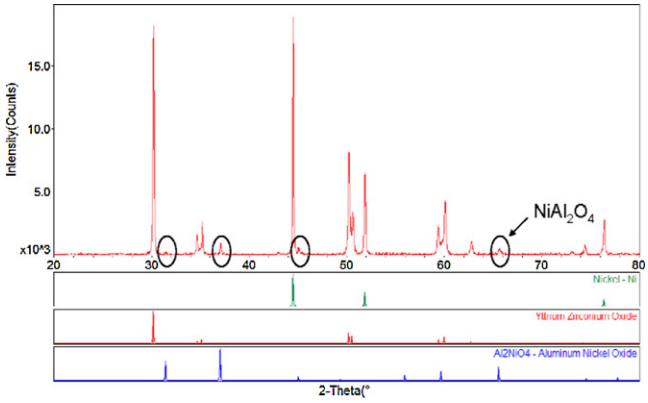

Fig. 4. XRD patterns of sintered anode support material $(Ni–YSZ)_{0.95}(Al_2O_3)_{0.05}$.

Fig. 4 shows the X-ray diffraction (XRD) patterns of the sintered $(Ni–YSZ)_{0.95}(Al_2O_3)_{0.05}$ specimen. The positions of the XRD peaks for Al_2O_3-doped Ni–YSZ specimens were unchanged, which suggested that the doping of Al_2O_3 did not lead to phase transformation. However, the diffraction peaks for Al_2NiO_4 formed.

The purpose of the lost-weight experiment after H_2 reduction is to determine the amount of Al_2O_3 that transformed to $NiAl_2O_4$ in the samples. The content of unreacted Al_2O_3 was calculated by the following equations:

$$N_{NiOU} = \frac{(m_{UR} - m_R)}{M_O} \quad (8)$$

$$N_{NiAl_2O_4} = N_{NiO} - N_{NiOU} \quad (9)$$

$$P = 1 - \frac{N_{NiAl_2O_4}}{N_{Al_2O_3}} \quad (10)$$

where N_{NiOU}, N_{NiO}, $N_{NiAl_2O_4}$ and $N_{Al_2O_3}$ refer to the number of moles of unreduced NiO, added NiO, $NiAl_2O_4$ and added Al_2O_3, respectively, m_{UR} and m_R refer to the mass of unreduced and reduced samples, respectively, M_O is the molar mass of O_2 and P is the content of unreacted Al_2O_3.

As shown in Fig. 5, there are 15 ± 5 wt% Al_2O_3 did not react with NiO to form $NiAl_2O_4$ in various samples. In Figs. 4 and 5, four phases were observed in the Al_2O_3-doped samples before and after H_2 reduction: the NiO, YSZ, $NiAl_2O_4$ and Al_2O_3 phases were observed before H_2 reduction; Ni, YSZ, $NiAl_2O_4$ and Al_2O_3 phases were observed after H_2 reduction.

Using Turner's equation (Eq. (7)) for multiple phases, the TECs of the samples before and after H_2 reduction were calculated by the following equation:

$$\alpha_c = \frac{\alpha_1 V_1 k_1 + \alpha_2 V_2 k_2 + \alpha_3 V_3 k_3 + \alpha_4 V_4 k_4}{V_1 k_1 + V_2 k_2 + V_3 k_3 + V_4 k_4} \quad (11)$$

where α_c, α_1, α_2, α_3 and α_4 are the TECs of the composite and the four phases before and after H_2 reduction, respectively, V_1, V_2, V_3 and V_4 are the volume fractions of the four phases and k_1, k_2, k_3 and k_4 are the values of the bulk modulus of the four phases.

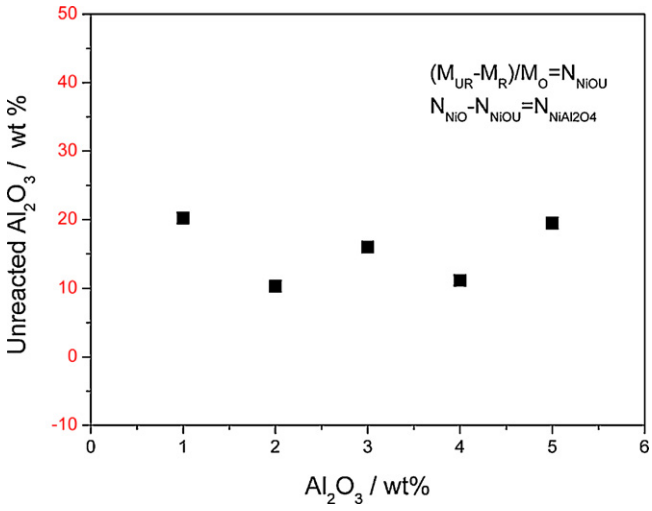

Fig. 5. The content of unreduced alumina in the anode support material $(NiO–YSZ)_{1-x}(Al_2O_3)_x$ as a function of total alumina content.

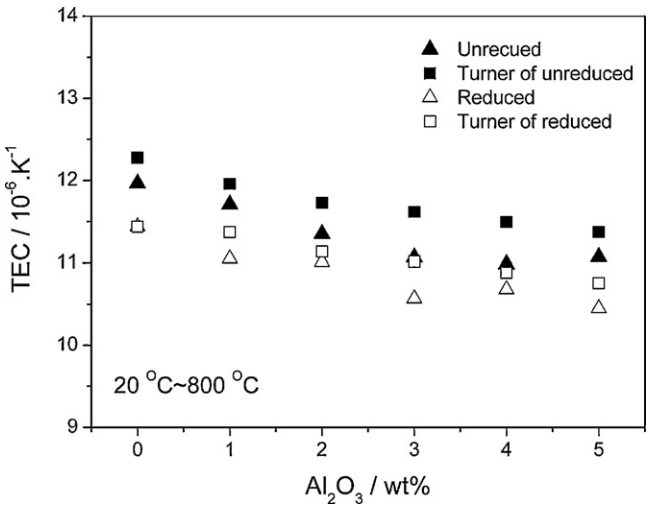

Fig. 6. Comparison of the measured TECs with those calculated by Turner's equation as a function of alumina content before and after reduction.

Table 3
Properties of the materials used in Eq. (11).

Properties	YSZ	Ni	$NiAl_2O_4$	Al_2O_3	NiO
E/GPa	220	207	265	350	277
$\alpha/10^{-6}\,K^{-1}$	10.50	13.30	8.41	8.00	13.80
$\rho/g\,cm^{-3}$	6.10	8.88	3.60	3.90	6.67
ν	0.31	0.31	0.34	0.23	0.31

The bulk modulus was calculated from Young's modulus by:

$$K = \frac{E}{3(1-2\nu)} \tag{12}$$

where K is the bulk modulus, E is the Young's modulus and ν is the Poisson's ratio.

The necessary values of Young's modulus, TEC, density and Poisson's ratio were taken from the literature and presented in Table 3 [16–19].

The reported values of TEC for the NiO–YSZ support and Ni–YSZ anode support materials varied considerably in the literature [1,15,20–22] and were compared with the present measurements in Table 4. Most of the literature results showed an increase in TEC when NiO was reduced to Ni. However, the work by Sun et al. [16] and this work showed a decrease in TEC as the volume fraction of solid YSZ increased because the volume of Ni was much smaller than that of NiO. The TEC values calculated by Turner's equation reduced slightly after the support was reduced in H_2. The properties of the composites were dependant on their microstructures. This might account for the variation in the values shown in Table 4.

The measured TEC values of the anode supports before and after H_2 reduction are compared in Fig. 6 and Table 5 with values calculated using Eq. (11). Each component in the composite was constrained to change dimensions with temperature, but their dimensions did not change at the same rate as the composite.

Table 4
Thermal expansion coefficient (presented in $10^{-6}\,k^{-1}$) for anode supports without alumina.

	NiO–YSZ	Ni–YSZ
This work	11.97	11.44
Turner's equation (11)	12.28	11.44
Literature [15]	12.82	12.53
Literature [20]	12.3	12.5
Literature [1,21]	12.1 [21]	12.6 [1]
Literature [22]	12.5	13.0

Table 5
Thermal expansion coefficient (presented in $10^{-6}\,k^{-1}$) for $(NiO–YSZ)_{1-x}(Al_2O_3)_x$ (x = 1–5 wt%).

	1 wt%	2 wt%	3 wt%	4 wt%	5 wt%
NiO–YSZ	11.71	11.35	11.07	10.99	11.07
Turner's equation (11)	11.96	11.73	11.62	11.49	11.37
Ni–YSZ	11.05	11.01	10.57	10.68	10.45
Turner's equation (11)	11.37	11.13	11.01	10.88	10.76

Therefore, the calculated values were slightly higher than the measured values, both before and after H_2 reduction. Nevertheless, the same tendency was observed with the measured and calculated values in that the addition of alumina and the formation of $NiAl_2O_4$ phase reduced the TEC of the support material. As shown in Table 5, the TECs decreased non-linearly with increasing alumina content before and after H_2 reduction. The TEC values of the samples were close to the TEC of 8YSZ ($10.8 \times 10^{-6}\,K^{-1}$) when the alumina content reached more than 2 wt% before H_2 reduction. After the $(Ni–YSZ)_{1-x}(Al_2O_3)_x$ samples with more than 2 wt% alumina were reduced in H_2 at 850 °C for 2 h, the TECs became less than $10.8 \times 10^{-6}\,k^{-1}$.

3.4. Effect of alumina on residual stresses in the electrolyte layer

The residual stresses at RT were estimated from the curvature of the laminate and the elastic constants of the individual layers. When tested by the residual stress tester, the sample surfaces were modified by Cu using electron beam evaporation to reflect the laser. The thickness of the YSZ layer and the anode were estimated from the cross-sectional SEM images as shown in Table 6. The residual stresses were calculated by Eq. (2).

Residual stress could also be calculated in the YSZ layer analytically according to the thermal misfit theory, expressed by:

$$\sigma^T = \frac{E_e\ \Delta\alpha\ \Delta T}{(1-\nu)} \tag{13}$$

Table 6
The thickness of the electrolyte layer (h_1) and the $(NiO–YSZ)_{1-x}(Al_2O_3)_x$ (x = 1–5 wt%) anode (h_2).

	0 wt%	1 wt%	2 wt%	3 wt%	4 wt%	5 wt%
h_1/μm	10.83	11.23	12.13	10.6	10.37	12.32
h_2/μm	420	420	440	420	440	440

Table 7
Residual stresses compared with literature values for anode supports without alumina.

Cell and test condition	Electrolyte residual stress/MPa	Thickness electrolyte/ μm	Thickness of anode substrate/mm
Oxidized RT	~512 [Eq. (2)]	10.83	0.42
Oxidized RT	~487 [Eq. (13)]		
Oxidized RT	~560 [7]	10	1.5
Oxidized RT	~660 [8]	20	2
Oxidized RT	~400 [23]	20	0.3
Oxidized RT	~600 [9]	10	0.51
Reduced RT	~223 [Eq. (2)]	10.83	0.42
Reduced	~268 [Eq. (13)]		
Reduced	~520 [7]	10	1.5
Reduced	~670 [8]	20	2
Reduced	~200 [23]	20	0.3
Reduced	~300 [9]	10	0.51

where E_e denotes Young's modulus of the electrolyte (YSZ, 220 GPa), $\Delta\alpha = \alpha_2 - \alpha_1$, and α_2 and α_1 denote the TECs of the anode material (Tables 4 and 5) and YSZ ($10.8 \times 10^{-6}\,k^{-1}$), respectively, ΔT denotes the temperature difference between the sintering temperature (1,350 °C) and room temperature (20 °C) and ν denotes the Poisson ratio (0.3).

For the anode support material NiO–YSZ without alumina, the RT residual stresses calculated by Eq. (2) were 512 MPa and 223 MPa before and after H_2 reduction, respectively. The values determined by the thermal misfit theory and the curvature method predicted that the residual stress of the electrolyte should decrease significantly after H_2 reduction. However, the results were qualitatively different from the literature values and only changed slightly. The room temperature stress level in the electrolyte of a 1.5-mm thick cell, as calculated using XRD method, was approximately 560 MPa for an oxidized anode substrate and 520 MPa for a reduced anode substrate [7]. Cells with slightly different anode geometry (2 mm thick) and electrolyte layer thickness (approximately 20–40 μm) had stresses in the same order of magnitude: 660 MPa for oxidized and flattened cells and 670 MPa for reduced cells [8]. Nevertheless, the results agreed very well with literature results [9,23] shown in Table 7. Cells have similar anode geometry (0.3–0.5 mm thick) and electrolate layer thickness (approximately 10–20 μm) with this work.

The effect of alumina and $NiAl_2O_4$ on the measured residual stresses of the electrolyte layer before and after H_2 reduction is demonstrated in Fig. 7. By the thermal misfit theory, the residual stress before H_2 reduction for the sample with more than 3 wt% alumina was only 20% of the sample without alumina. However, the residual stress was lower to 20% of the sample without alumina for the sample with more than 4 wt% alumina by the curvature method. The residual stresses in reduced samples were only 100 MPa when alumina was added, as shown in Fig. 7. No good agreement existed between the misfit theory and the curvature method when the residual stress was lower than 200 MPa, which might be affected by external stresses during fabrication. Other types of residual stresses in addition to the thermal misfit residual stress might be present during fabrication, which were estimated to be approximately 100 MPa according to the samples reduced with H_2. The decrease of residual stress was due to the decreased TEC of the anode-support material as alumina was added.

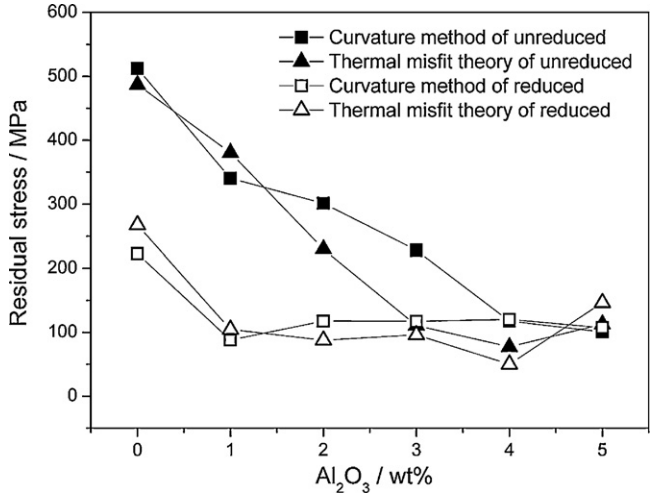

Fig. 7. Residual stresses measured by the curvature method and calculated by the thermal misfit theory as a function of alumina content before and after reduction.

4. Conclusions

The effects of Al_2O_3 on the curvature, Young's modulus, TEC and residual stress of the anode-support material $(NiO–YSZ)_{1-x}(Al_2O_3)_x$ (x = 1–5 wt%) are discussed in this paper. The addition of alumina flattened the half cell before and after H_2 reduction when it was fabricated under the same conditions as the half cell without alumina. The radius of curvature for the sample with 3 wt% alumina changed from 2.04 m to 2.18 m, which was the smallest change in this study.

When the alumina content was more than 2 wt% before reduction, the TECs of the samples were close to those of 8YSZ samples at $10.8 \times 10^{-6}\,k^{-1}$. The measured values were compared with values calculated by Turner's equation. Each component in the composite, which was constrained to change dimensions with temperature, did not change at the same rate as the composite. Therefore, the calculated values were slightly higher than the measured ones.

The decrease of residual stress was due to the decreased TEC of the anode-support material as alumina was added. The residual stress for the sample with more than 4 wt% alumina was only 20% of the residual stress for the sample without alumina before reduction. The residual stresses in reduced samples were only approximately 100 MPa after alumina was added.

Acknowledgements

This work was financially supported by the National High-Tech Research and Development Program of China (Program No. 863, Grant No. 2009AA05Z122), and in part by the National Natural Science Foundation of China (Grant No. 50902135) and the Ningbo Nature Science Foundation (Grant No. 2010A610149).

References

[1] N.Q. Minh, Journal of the American Ceramic Society 76 (1993) 563–588.
[2] M. Dokiya, Solid State Ionics 152 (2002) 383–392.
[3] F. Zhao, A.V. Virkar, Journal of Power Sources 141 (2005) 79–95.
[4] A.C. Muller, D. Herbstritt, E. Ivers-Tiffee, Solid State Ionics 152 (2002) 537–542.
[5] Z.R. Wang, J.Q. Qian, S.R. Wang, J.D. Cao, T.L. Wen, Solid State Ionics 179 (2008) 1593–1596.
[6] M. Radovic, E. Lara-Curzio, Acta Materialia 52 (2004) 5747–5756.
[7] W. Fischer, J. Malzbender, G. Blass, R.W. Steinbrech, Journal of Power Sources 150 (2005) 73–77.
[8] H. Yakabe, Y. Baba, T. Sakurai, Y. Yoshitaka, Journal of Power Sources 135 (2004) 9–16.
[9] E. Lara-Curzio, Core Technology Peer Review Workshop, Tampa, FL, USA, 01/27/2005–01/28/2005, 2005.
[10] J. Malzbender, T. Wakui, R.W. Steinbrech, Fuel Cells 6 (2006) 123–129.
[11] GB/T 10700-2006.
[12] A.G. Evans, J.W. Hutchinson, Acta Metallurgica et Materialia 43 (1995) 2507–2530.
[13] A. Selcuk, A. Atkinson, Journal of the European Ceramic Society 17 (1997) 1523–1532.
[14] M. Pihlatie, A. Kaiser, M. Mogensen, Journal of the European Ceramic Society 29 (2009) 1657–1664.

[15] T.H. Nam, G. Requena, P. Degischer, Composites Part a-Applied Science and Manufacturing 39 (2008) 856–865.
[16] B. Sun, R.A. Rudkin, A. Atkinson, Fuel Cells 9 (2009) 805–813.
[17] N.M. Sammes, Y.H. Du, Journal of Materials Science 38 (2003) 4811–4816.
[18] Z. Hashin, S. Shtrikman, Journal of the Mechanics and Physics of Solids 11 (1963) 127–140.
[19] M. Lieberthal, W.D. Kaplan, Materials Science and Engineering a-Structural Materials Properties Microstructure and Processing 302 (2001) 83–91.
[20] N.Q. Minh, T. Takahashi, Science and Technology of Ceramic Fuel Cells, Elsevier, Amsterdam, The Netherlands, 1995.
[21] M. Mori, T. Yamamoto, H. Itoh, H. Inaba, H. Tagawa, Journal of the Electrochemical Society 145 (1998) 1374–1381.
[22] J. Malzbender, W. Fischer, R.W. Steinbrech, Journal of Power Sources 182 (2008) 594–598.
[23] H. Sumi, K. Ukai, M. Yokoyama, Y. Mizutani, Y. Doi, S. Machiya, Y. Akiniwa, K. Tanaka, Journal of Fuel Cell Science and Technology 3 (2006) 68–74.